Polyphase–Discrete Fourier Transform Spectrum Analysis for the Search for Extraterrestrial Intelligence Sky Survey

G. A. Zimmerman
Communications Systems Research Section

S. Gulkis
Space Physics and Astrophysics Section

The sensitivity of a matched filter-detection system to a finite-duration continuous wave (CW) tone is compared with the sensitivities of a windowed discrete Fourier transform (DFT) system and an ideal bandpass filter-bank system. These comparisons are made in the context of the NASA Search for Extraterrestrial Intelligence (SETI) microwave observing project (MOP) sky survey. A review of the theory of polyphase-DFT filter banks and its relationship to the well-known windowed-DFT process is presented. The polyphase-DFT system approximates the ideal bandpass filter bank by using as few as eight filter taps per polyphase branch. An improvement in sensitivity of ~3 dB over a windowed-DFT system can be obtained by using the polyphase-DFT approach. Sidelobe rejection of the polyphase-DFT system is vastly superior to the windowed-DFT system, thereby improving its performance in the presence of radio frequency interference (RFI).

I. Introduction

The Search for Extraterrestrial Intelligence (SETI) sky survey will use a spectrum-analysis system with a 640-MHz total bandwidth and 33,554,432 (2^{25}) channels divided equally between two 320-MHz-wide polarizations [1]. The purpose of the system is to detect finite-duration continuous wave (CW) tones. Cost and technology constrain the number of channels in the system. To evaluate the resulting sensitivity loss, a study was undertaken of the relative sensitivities of theoretically optimal detection and systems with a fixed number of channels.

Spectrum analysis by means of a windowed discrete Fourier transform (DFT), usually implemented as a fast Fourier transform (FFT), is used in a wide variety of fields [2]. For the SETI sky survey, as in many appli-

cations, a windowed DFT has been proposed to channelize the input bandwidth [3]. The windowed DFT isolates interference in the frequency domain and allows CW signal-detection algorithms to operate on the narrowband output channels of the DFT, which improves the signal-to-noise ratio (SNR) at which signal detection must take place. However, the superior sidelobe rejection of windowed DFT's does not come without a performance penalty. This penalty is well-known and is tabulated in [2] for various window functions. For most common window functions, the worst-case processing loss is between 3 to 4 dB. For the SETI sky survey, this loss would add to that incurred by fixing the number of channels. Recovering this processing loss would be equivalent to halving the system temperature or doubling the antenna's collecting area.

A multirate digital signal-processing technique, known as a polyphase-DFT filter bank, is proposed to recover most of the windowed-DFT processing loss while providing superior interference isolation. The theory of polyphase-DFT filter banks has been established in the multirate digital-signal-processing community for some years now. However, unlike windowed-DFT techniques, the filter bank theory is not, in general, well-known. It is the intent of this article to propagate the theory of polyphase-DFT filter banks as a technique related to the use of windows with DFT's, and it is suggested that applications using windowed DFT's might benefit by switching to polyphase-DFT filter banks.

The first part of this article compares the sensitivity of the theoretically optimal matched filter-detection system with the sensitivities of a Hanning windowed-DFT system and an ideal bandpass filter-bank system. The second part reviews the theory of polyphase-DFT filter banks and their relation to windowed DFT's. In the third part, the performance of simple polyphase-DFT filter preprocessing is examined.

II. Comparative Sensitivities

The best possible sensitivity that can be expected with the SETI sky survey will be achieved in the absence of radio frequency interference (RFI) with the use of a matched filter detector [4]. It is therefore of interest to calculate the matched filter-detection system sensitivity and use that as a standard to judge how well the SETI sky survey compares with the optimum. The flux sensitivity that can be achieved with a matched filter system is given in this section. This sensitivity is also compared with two systems with the same fixed number of channels: a Hanning windowed-DFT system of 30-Hz resolved equivalent noise bandwidth and an ideal bandpass filter bank of 20-Hz resolved bandwidth.

The SETI sky survey will sweep at a constant angular rate on the sky with a DSN 34-m high-efficiency (HEF) antenna. As the antenna transits a source on the sky, the source will be convolved by the antenna's beam shape. For this analysis, the authors assume that the antenna pattern sweeping past a CW point source can be approximated by a square-wave pulse of width equal to the half-power beamwidth (HPBW) of the antenna. The SNR for a matched filter system is then given by

$$SNR = \frac{A\phi\tau}{kT}$$

where A is the effective area of the antenna, ϕ is the received flux, τ is the approximate time to move the telescope one HPBW, and kT is the spectral noise density of the receiver and background. Most of these are system parameters. The authors assume a 34-m diameter antenna with a 60-percent effective collecting area and a system temperature of 25 K. The telescope is assumed to be driven at a constant rate of 0.2 deg per second across the sky. The constant scan rate gives a pulse duration, and hence a resolved matched filter bandwidth, which varies with frequency. The pulse duration time is approximately $\tau = 3/\nu$ sec, when ν is expressed in GHz.

To determine the minimum detectable flux density, one must first determine the minimum detectable SNR. Two factors determine the SNR required for a detection by the SETI sky survey. The first is a requirement limiting to 0.1 the probability of missing a signal. This parameter is the same for both the matched filter system and any system with a fixed number of channels. The second parameter required to determine the detectable SNR is the probability of false alarm (P_{FA}). Since a detection implies that a sky location and frequency should be reobserved, the amount of available look-back time is the main constraint on this parameter. The SETI sky survey requirement on P_{FA} is formulated as 3,000 hits per 320-MHz survey over the entire sky. Since the antenna beamwidth varies with frequency, the number of resolvable points on the sky increases as the square of the frequency, decreasing the required P_{FA} inversely in the same manner. Since the matched filter system has a resolved bandwidth that varies with frequency, the number of matched filter channels in a 320-MHz survey varies inversely with frequency. As a result, the required P_{FA} for the matched filter system decreases approximately inversely with frequency, while the required P_{FA} for a system with a fixed number of channels

per bandwidth decreases as the inverse square of the frequency. There is, therefore, considerably more variation in the SNR required for detection for a system with a fixed number of channels than for a matched filter system.

Having defined the SNR's required for detection, as well as the effective area, the system temperature, and the pulse duration, the flux sensitivity ϕ can be computed. The matched filter system sensitivity can be straightforwardly calculated, as can the sensitivity for an ideal bandpass filter system, given a fixed number of channels. A windowed DFT system, however, has additional losses that must be considered if the signal-detection process is to be performed independently on individual DFT-channel outputs. A windowed DFT has two sources of loss relative to an ideal bandpass filter bank with identical channel spacing. These are shown in Fig. 1. The first is an expansion of the equivalent noise bandwidth of a DFT channel relative to the channel spacing. This loss is independent of the position of a signal within the DFT channel, and is approximately 1.76 dB for Hanning windowed DFT's. The second loss, commonly called "scallop loss," is due to the transfer function of a DFT bin. The scallop loss is dependent on the position of a signal within the DFT channel and varies from no loss to 1.42 dB, worst case, in the Hanning windowed DFT.

The sensitivities of the three systems can now be computed and are shown in Fig. 2. Losses of the ideal bandpass filter-bank system and the worst-case Hanning windowed DFT system are shown in Fig. 3. A number of conclusions can be drawn from these calculations. First, a sky survey with a fixed number of channels ranges from 1.9 to 7.5 dB less sensitive than the theoretical optimum. Second, the windowed-DFT approach is approximately 3 dB less sensitive than an ideal bandpass filter bank with the same channel spacing. Recovering the loss due to the windowed DFT would reduce the maximum loss of the sky survey relative to the optimum to approximately 4.5 dB. The authors therefore present an approximation to an ideal bandpass filter bank.

III. Polyphase-DFT Filter Banks

Consider a bank of K filters based on the same lowpass prototype impulse response $h(n)$, each centered at a different center frequency, $\omega_k = 2\pi k/K, k = 0, 1, \ldots, K-1$. Since the filters share the same prototype impulse response, but are just shifted in frequency by ω_k, the impulse response of each is simply $h_k(n) = h(n)e^{j\omega_k n}$, and all have identically shaped passbands (centered at different frequencies, of course). Let

$$y_k(n) = \sum_{p=1}^{KN_t} x(n-p)h_k(p), \quad h_k(n) = h(n)e^{j2\pi kn/K}$$

where KN_t is the length of the finite-impulse response filter $h(n)$. Note that if the $h(n)$ prototype filter is an ideal lowpass filter, with a passband $-\pi/K < \omega < \pi/K$, then this arrangement covers the spectrum with no losses and no overlapping bins. Furthermore, if the output is decimated K:1, as in Fig. 4, then there is no oversampling.

Let $p = \ell k - i; \quad i = 0, 1, \ldots, K-1$, and consider the K:1 decimated outputs of the filters so that $n = mK$. Then

$$y_k(mK) = \sum_{i-0}^{K-1} \sum_{\ell=1}^{N_t} x\left[(m-\ell)K + i\right] h_k(\ell K - i)$$

Keep in mind that only one out of every K samples from each filter h_k is selected. It is apparent that the output recognizes only a given input sample multiplied by every Kth filter coefficient. The subset of the filter coefficients that multiplies a given input data point depends on the phase of the input data point relative to the K:1 decimation. To represent the double summation form above, the authors introduce the polyphase filter structure for the decimated filter h_k shown in Fig. 5. The ith polyphase branch of the decimated filter h_k is $\overline{p}_{i,k}$, defined as: $\overline{p}_{i,k}(m) = h_k(mK - i) i = 0, 1, \ldots, K-1$, and the branch input signals are $x_i(m) = x(mK + i)$.

Now, since $h_k(n) = h(n)e^{j(2\pi k/Kn)}$:

$$\begin{aligned}\overline{p}_{i,k}(m) = h_k(mK-i) &= h(mK-i)e^{j(2\pi k/K)}e^{-j\omega_k i} \\ &= h_k(mK-i)e^{j\omega_k i} = \overline{p}_{i,0}(m)e^{-j\omega_k i}; \\ & i, k = 0, 1, \ldots, k-1\end{aligned}$$

Note that all the filters are now defined in terms of outputs of the prototype filter's polyphase implementation. Hence:

$$y_k(mK) = \sum_{i=0}^{K-1} e^{-j(2\pi ki/K)} \sum_{l=1}^{N_t} x_i(m-\ell)\overline{p}_{i,0}(\ell)$$

For ease of notation, define $\overline{p}_i(m) = \overline{p}_{i,0}(m)$, and call the outputs of these prototype filter polyphase branches $z_i(m)$, where i is the polyphase branch number. The resulting structure for filter h_k (centered at ω_k) is shown in Fig. 6.

The output is clearly: $y_k(m) = \sum_{i=0}^{K-1} z_i(m)e^{-j\omega_k i}$, which is bin k of the DFT of the z_i's for a fixed m over the branch index i. Since the z_i's are the same for all K filters $h_k, k = 0, 1, \ldots, K-1$, the entire bank can be synthesized by computing the z_i's and taking the DFT, as shown in Fig. 7.

In summary, by designing one lowpass filter of length $N = K(N_t)$ taps and dividing it up into K polyphase branches of N_t taps each, and by applying a K-point DFT to their outputs as shown above, one can synthesize a filter bank of equally spaced (on the DFT-bin center frequencies), identically shaped filters.

This concludes the derivation of the filter-bank structure; a more detailed explanation can be found in [5]. In Chapter 3, sections 3.3.2 and 3.3.3 of [5], Crochiere and Rabiner derive polyphase structures in general, and in Chapter 7, sections 7.2.1, 7.2.2, and 7.2.3, they describe uniform DFT filter banks for the "critically sampled" (number of filter bands, K = decimation factor) case described here. An alternative derivation of the polyphase-DFT filter bank can be constructed by using an inverse DFT and a counterclockwise commutation of the input data points. An advantage of the forward-DFT approach is that the first polyphase branch to receive a data point each commutator cycle also provides the first data point to the DFT. In the inverse DFT approach, the first data point of the sequence on which the inverse DFT is to be performed is provided by the last polyphase branch to receive its input. This data ordering can be important in the design of real-time signal processors.

The additional processing necessary to produce a polyphase-DFT filter bank from a DFT is a separable, preprocessing step, similar to multiplication by a time-domain window function in the windowed DFT. In fact, the windowed DFT is a special, degenerate case of a polyphase-DFT filter bank. Consider the case where $N_t = 1$, then the prototype filter is of the same length as the DFT. The structure then becomes, in fact, an ordinary windowed DFT, with the window function being the set of filter coefficients.

$$[z_i(m) = h(i)\ \chi(mK + i)]$$

Since the polyphase structure is just a front-end process to a DFT, a polyphase system with programmable filter coefficients can easily be changed into a simple windowed DFT. This is accomplished by setting all the coefficients to zero except for one tap per polyphase branch, e.g., all except tap 1 of each branch. Furthermore, any finite impulse response (FIR) polyphase-DFT filter bank can conceptually be converted to an equivalent windowed DFT as follows:

(1) Take the samples of the impulse response of the prototype lowpass filter as the window coefficients.

(2) Perform an N_tK-point windowed DFT by using consecutive time samples.

(3) Take only the outputs of bins whose indexes are integer multiples of N_t, i.e., bins $N_t, 2N_t, 3N_t, \ldots$, and discard the other bin outputs.

(4) Continue performing steps 2 and 3, and shift the start of the input sequence to the windowed DFT by K samples each time so that the first DFT is on samples $x(0)$ to $x[N_t(K-1)]$, the second DFT is on samples $x(K)$ to $x[(N_t+1)(K-1)]$, and the ith DFT is on samples $x[(i-1)K]$ to $x\{[N_t+(i-1)](K-1)\}$.

The reader will notice that while this method produces the same output as the polyphase-DFT filter bank, it requires, in general, a large amount of computation to do so, and is not a recommended approach.

IV. Performance of Polyphase-DFT Filter Banks

Examples of polyphase-DFT filter-bank performance appear in Table 1. Note that the total number of inputs (the time aperture) affecting each output is KN_t samples; however, for a fixed resolution in absolute frequency (hertz), the prototype lowpass filter $h(n)$ must approximate a truncated sync function whose major weighting (main lobe, between the -1 and $+1$ nulls) is of a *fixed time duration* proportional to the reciprocal of the desired lowpass bandwidth. Hence, the impulse response of this longer time aperture looks and acts like an ideal lowpass filter with a truncated time aperture. The advantage of this longer time aperture is that it allows the filter-transfer function to have a flatter passband and sharper transition, which provides both increased sensitivity to desired signals as well as increased interference immunity. An example of an $N_t = 8$-tap polyphase-filter transfer function versus a Hanning windowed transfer function is shown in Fig. 8.

Some quick filter designs, with Parzen (Riesz) windowed lowpass filters, produced the following worst-case processing losses, as defined by Harris [2]:

Worst-Case Loss (dB)

$$= 10 \log \left[\frac{\text{Equivalent Noise Bandwidth}}{\text{Input Bandwidth/Number of Channels}} \right]$$

$$+ \text{Minimum Gain } (\pm 0.5 \text{ bins offset})$$

As usual with digital FIR filter design, optimization can be performed to trade off sidelobe levels for worst-case losses. Transfer functions for these filter designs are shown in Figs. 9–16. Table 2 shows sample responses for these Parzen smoothed lowpass filters.

Computationally the N_t-tap polyphase structure requires N_t multiplications and $N_t - 1$ additions per real data-point input. In comparison, a K-point radix-2 fast Fourier transform (FFT) requires $1.5(\log_2 K)$ real additions and $\log_2 K$ real multiplications, for a total of $2.5(\log_2 K)$ operations per real data-point input. A 12-tap filter is, therefore, slightly less computationally intensive than a 1,024-point radix-2 FFT. For large FFT systems, such as the SETI sky survey system, the polyphase-DFT filter bank offers a method of significantly improving the system with a relatively small computational increase. However, since the polyphase preprocessing stage must store N_t vectors, each of which is the length of the FFT to be performed, the memory requirements for a large polyphase-DFT filter bank, such as SETI's, can be significant. The required data storage for a K-channel filter bank is $N_t K$ times the input word length. For a 4-Mchannel filter bank with 8-bit complex inputs, such as SETI's, this results in $8N_t$ Mbytes of memory just for data. In addition, filter coefficients must be stored, but these can often take advantage of symmetries and simple data-compression techniques.

V. Conclusions

Like the application of a window to the sequence prior to the DFT in windowed DFT's, the additional processing involved in polyphase-DFT filter banks is a preprocessor to the conventional DFT. In fact, the conventional windowed DFT is the simplest case of a polyphase-DFT filter bank. Moreover, the polyphase-DFT filter bank can operate on a time aperture larger than the conventional DFT. As a result, it is possible to easily synthesize DFT-bin (window) transfer functions with significantly less frequency-scallop loss, less noise-bandwidth expansion, and faster sidelobe falloff than is possible with conventional windowed-DFT techniques. Furthermore, the computational cost is generally minimal as compared with that of the DFT. For example, the computational cost of a 64-point radix-2 FFT produces a transfer function with a worst-case processing loss of 1 dB, as defined by Harris in his analysis of windows [2]. The best windows in [2] have a worst-case loss of 3 dB. By recovering much of the processing loss inherent in windowed-DFT spectrum analysis as well as providing superior isolation of narrowband interference, polyphase-DFT spectrum analysis provides a relatively inexpensive means for the SETI sky survey to increase its sensitivity by at least 2 dB, which provides a sensitivity that ranges between 2.9 to 5.5 dB from optimal.

References

[1] G. A. Zimmerman, B. Charny, M. F. Garyantes, and M. J. Grimm, "A 640-MHz 32-Megachannel Real-Time Polyphase-FFT Spectrum Analyzer," *TDA Progress Report 42-107*, vol. October–December 1991, Jet Propulsion Laboratory, Pasadena, California, pp. 132–140, November 15, 1991.

[2] F. Harris, "On the Use of Windows for Harmonic Analysis with the Discrete Fourier Transform," *Proceedings of the IEEE*, vol. 66, no. 1, pp. 51–83, January 1978.

[3] M. P. Quirk, H. C. Wilck, M. F. Garyantes, and M. J. Grimm, "A Wideband, High-Resolution Spectrum Analyzer," *TDA Progress Report 42-93*, vol. January–March 1988, Jet Propulsion Laboratory, Pasadena, California, pp. 188–198, May 15, 1988.

[4] B. Oliver, "Parametric Relations in a Full Sky Search," *NASA SP 419*, NASA, Washington, D.C., p. 129, 1977.

[5] R. Crochiere and L. Rabiner, *Multirate Digital Signal Processing*, Prentice-Hall Signal Processing Series, Englewood Cliffs, New Jersey: Prentice-Hall, 1983.

Table 1. Examples of polyphase-DFT filter-bank performance

Taps per branch, N_t	Worst-case processing loss, dB	Interference rejection: offset bins to >70-dB attenuation
2	2.503	7
4	1.513	4
6	1.236	3
8	1.048	3
12	0.653	2
16	0.543	2

Table 2. Sample responses for Parzen smoothed lowpass filters

Taps per branch, N_t	Min. gain at 0.5 bin, dB	Equivalent noise bandwidth, bins/Hz	Min. gain, dB	Worst-case loss, dB
2	−0.492	1.589/30.302	−0.492	2.503
4	−0.244	1.335/25.460	−0.258	1.513
6	−0.128	1.239/23.638	−0.304	1.236
8	−0.077	1.184/22.581	−0.315	1.048
12	−0.295	1.083/20.649	−0.308	0.653
16	−0.252	1.058/20.181	−0.298	0.543
1[a]	−3.908	1.016/19.372		3.976
1[b]	−1.423	1.516/28.908		3.229

[a] Rectangular window.
[b] Hanning window.

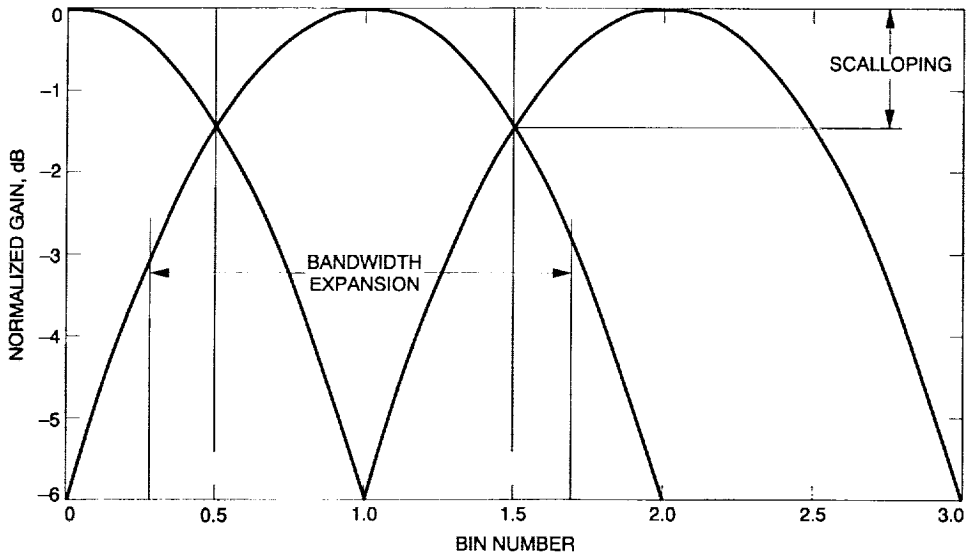

Fig. 1. Losses in Hanning windowed discrete Fourier transforms (DFTs).

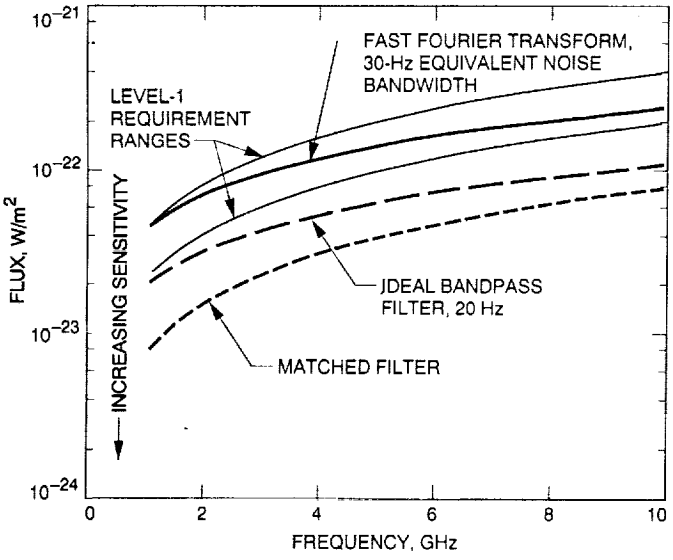

Fig. 2. A comparison of system sensitivities.

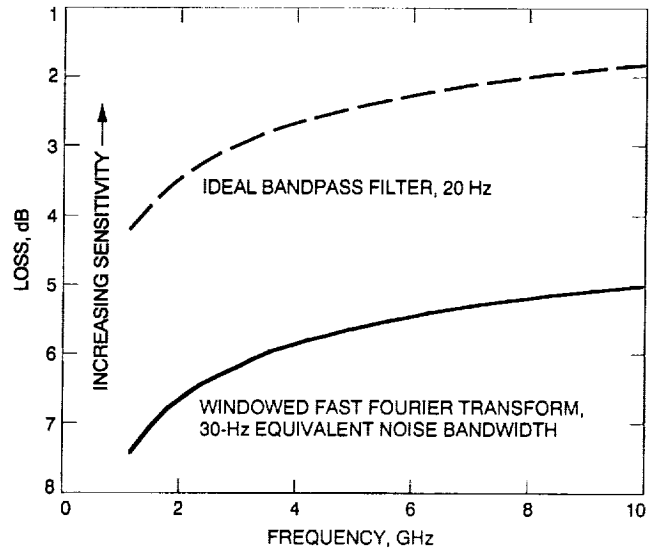

Fig. 3. A comparison of losses relative to the theoretical optimum.

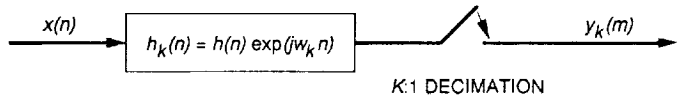

Fig. 4. A *K*:1 decimated bandpass filter from a lowpass prototype.

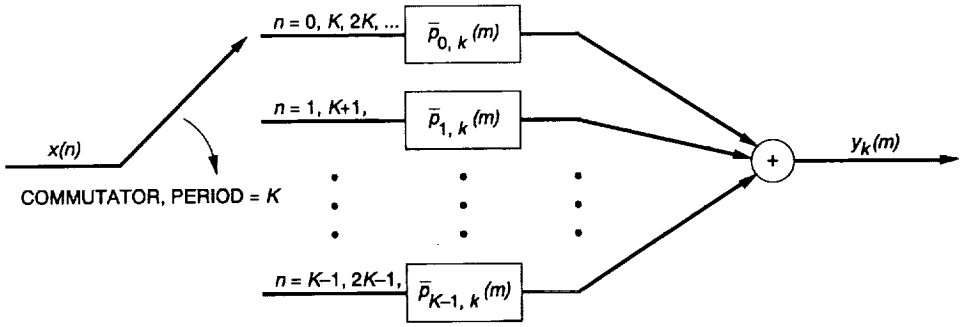

Fig. 5. General polyphase structure for the K:1 decimated filter h_k.

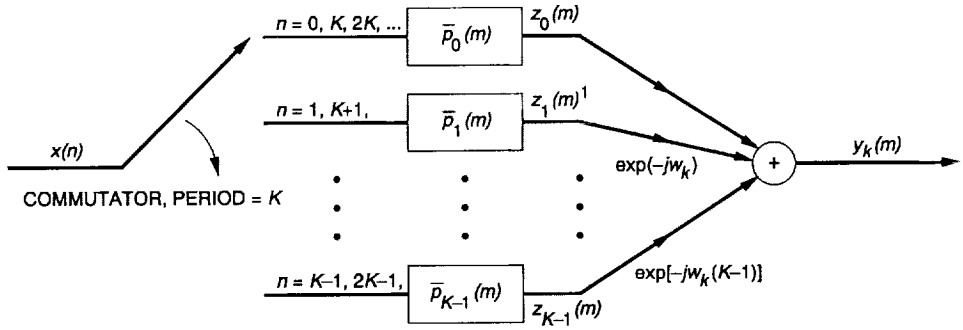

Fig. 6. Polyphase structure for the kth K:1 decimated filter h_k, with center frequency $\omega_k = 2\pi k/K$.

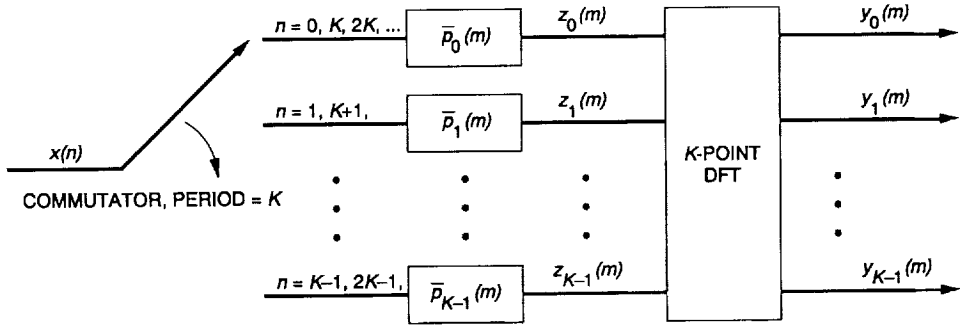

Fig. 7. Discrete Fourier transform implementation for a bank of identically spaced, identically shaped filters.

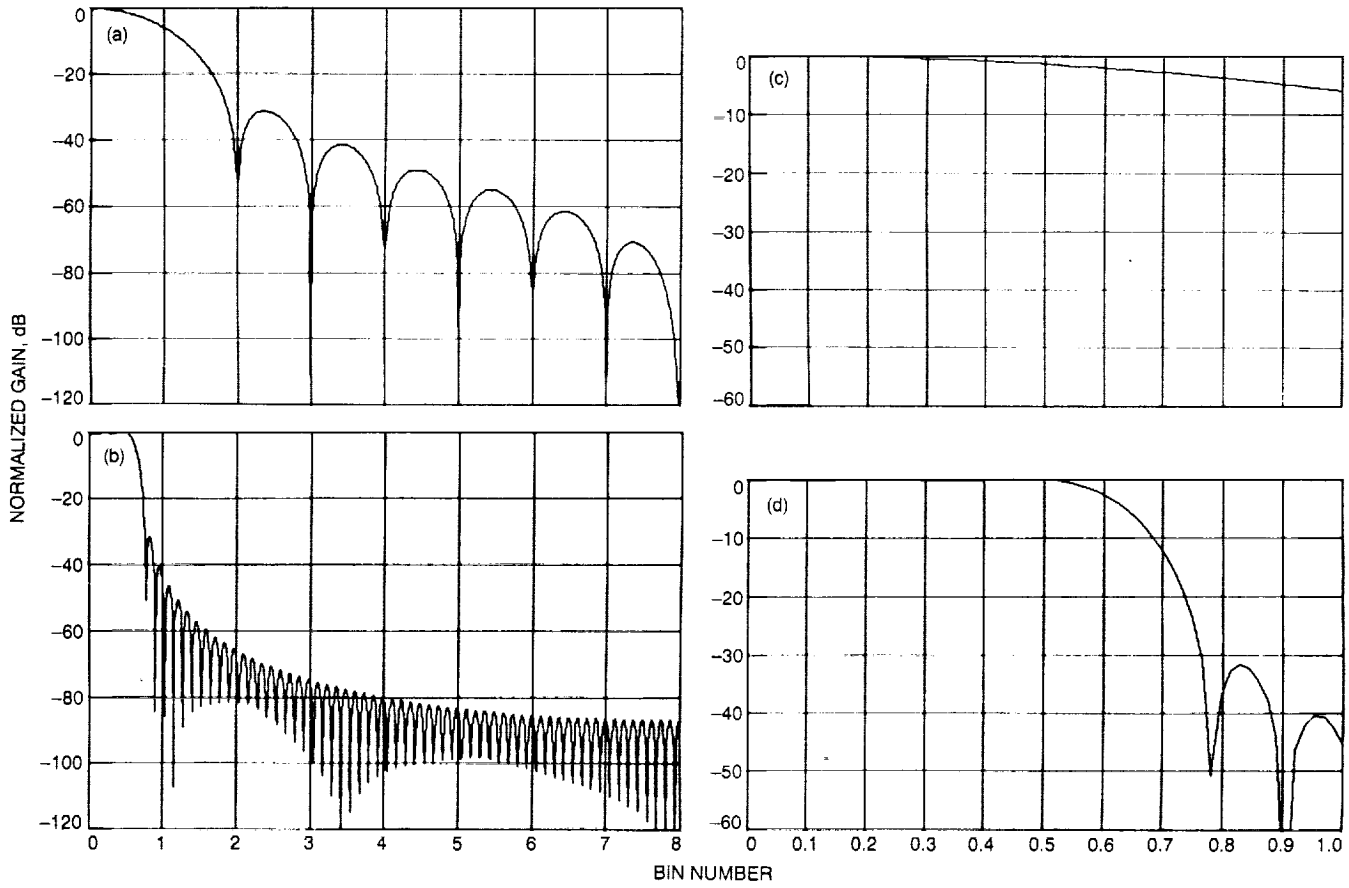

Fig. 8. A comparison of a Hanning windowed discrete Fourier transform with an 8-tap polyphase discrete Fourier transform: (a) Hanning window; (b) 0.65-bin lowpass filter, Parzen smoothed; (c) Hanning window, close up; and (d) 0.65-bin lowpass filter, Parzen smoothed, close up.

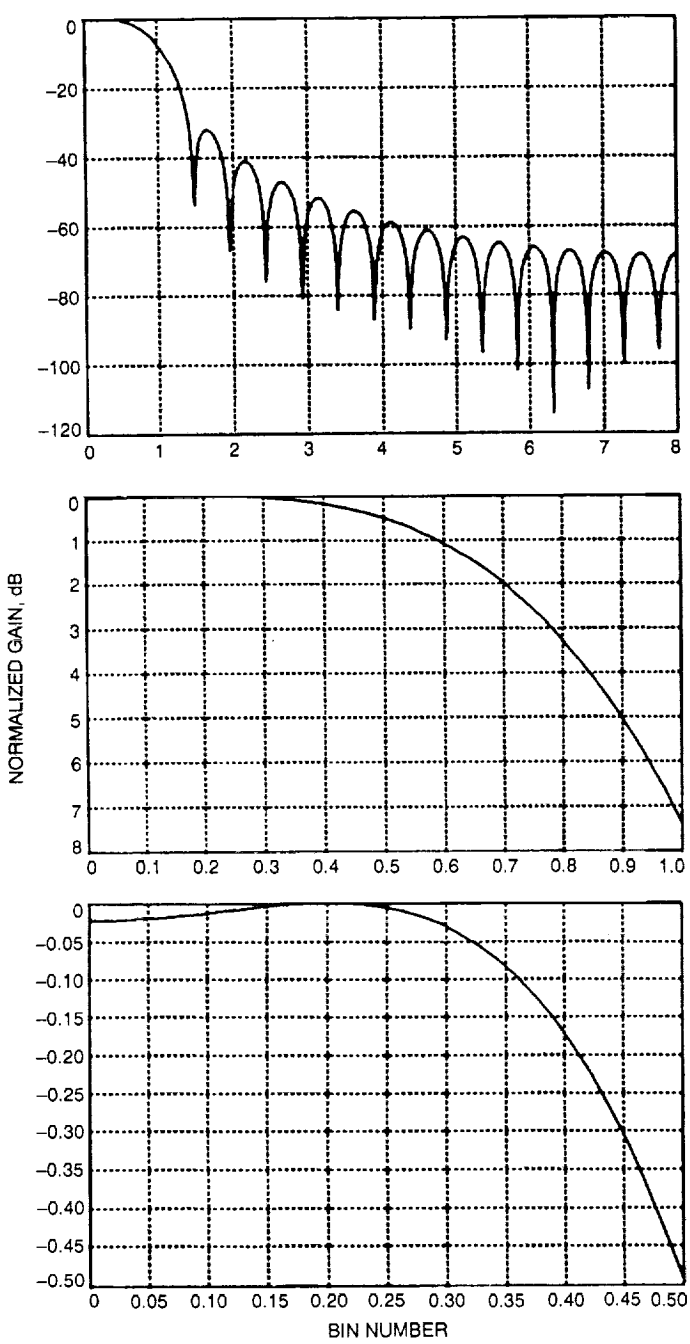

Fig. 9. Sample response with two close-up views of a 2-tap, 0.95-bin Parzen smoothed lowpass filter.

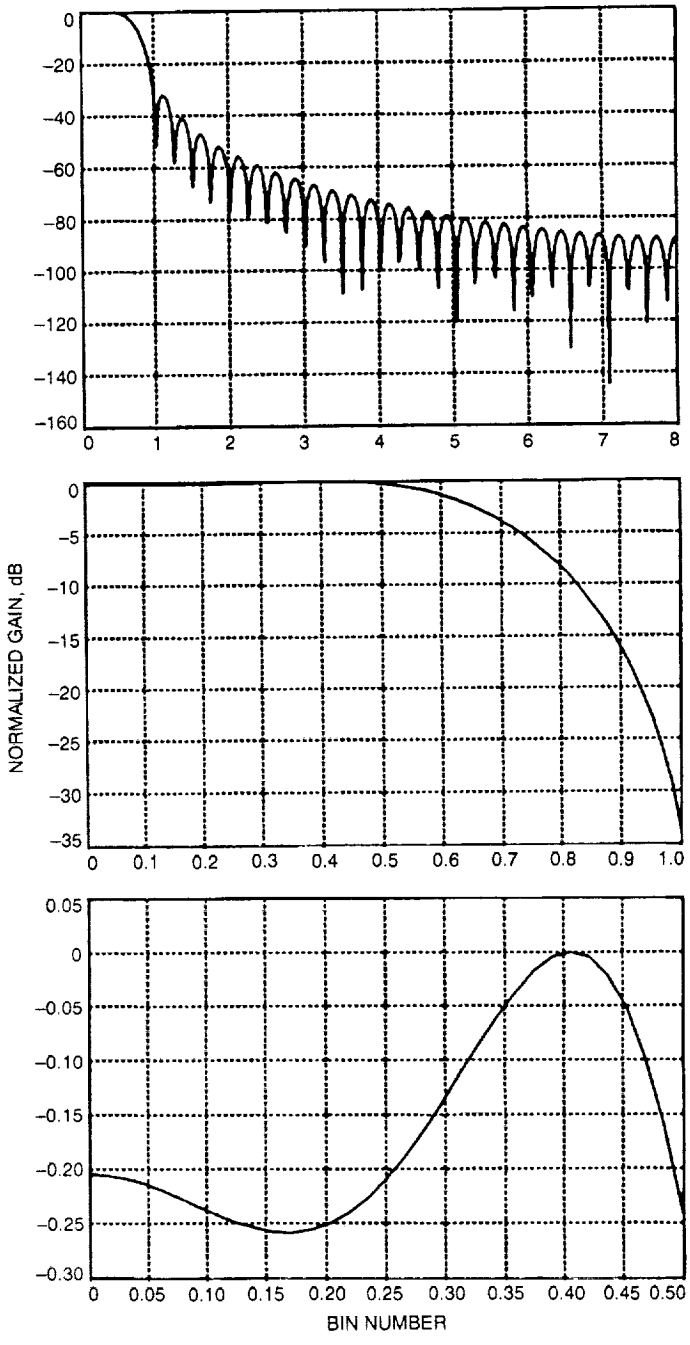

Fig. 10. Sample response with two close-up views of a 4-tap, 0.76-bin Parzen smoothed lowpass filter.

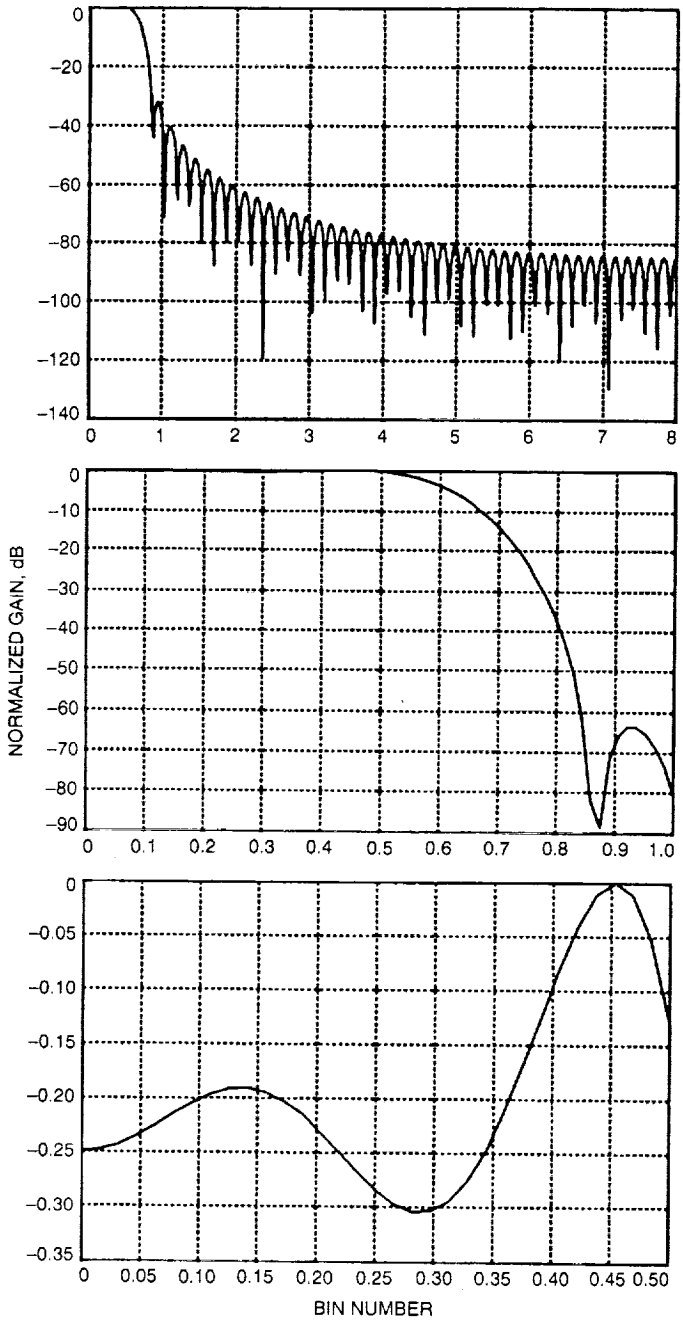

Fig. 11. Sample response with two close-up views of a 6-tap, 0.69-bin Parzen smoothed lowpass filter.

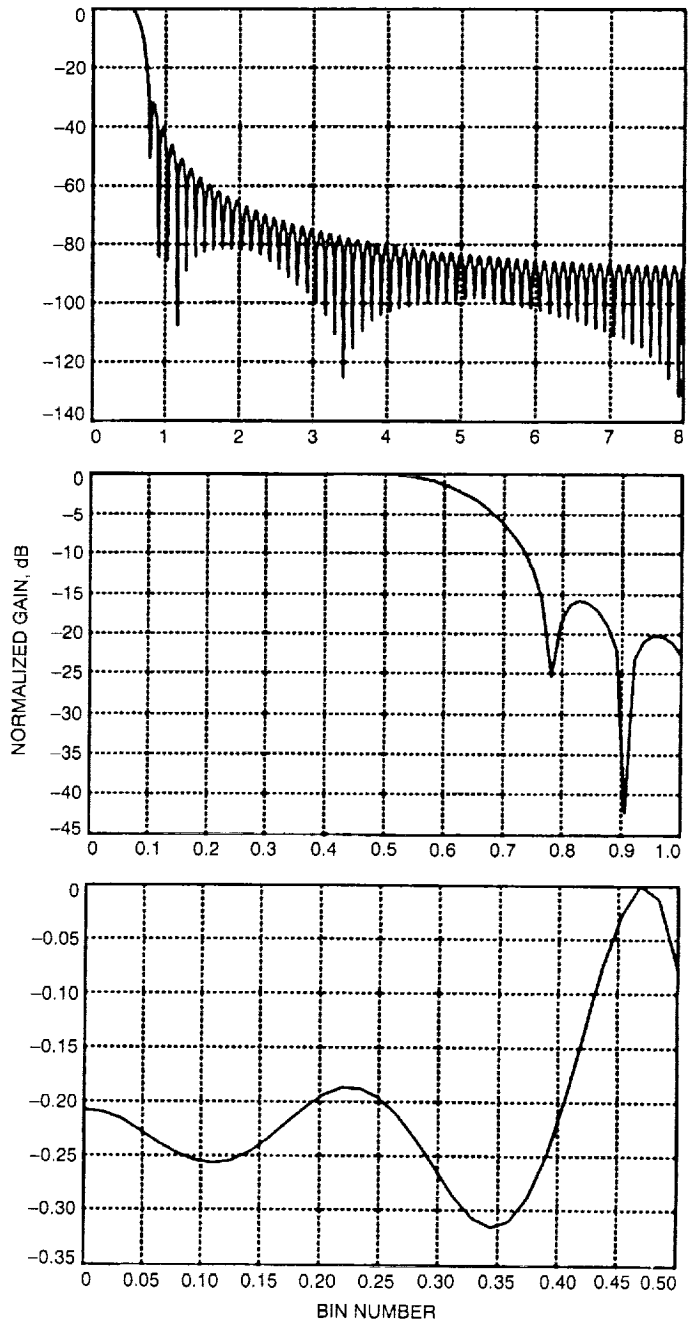

Fig. 12. Sample response with two close-up views of an 8-tap, 0.65-bin Parzen smoothed lowpass filter.

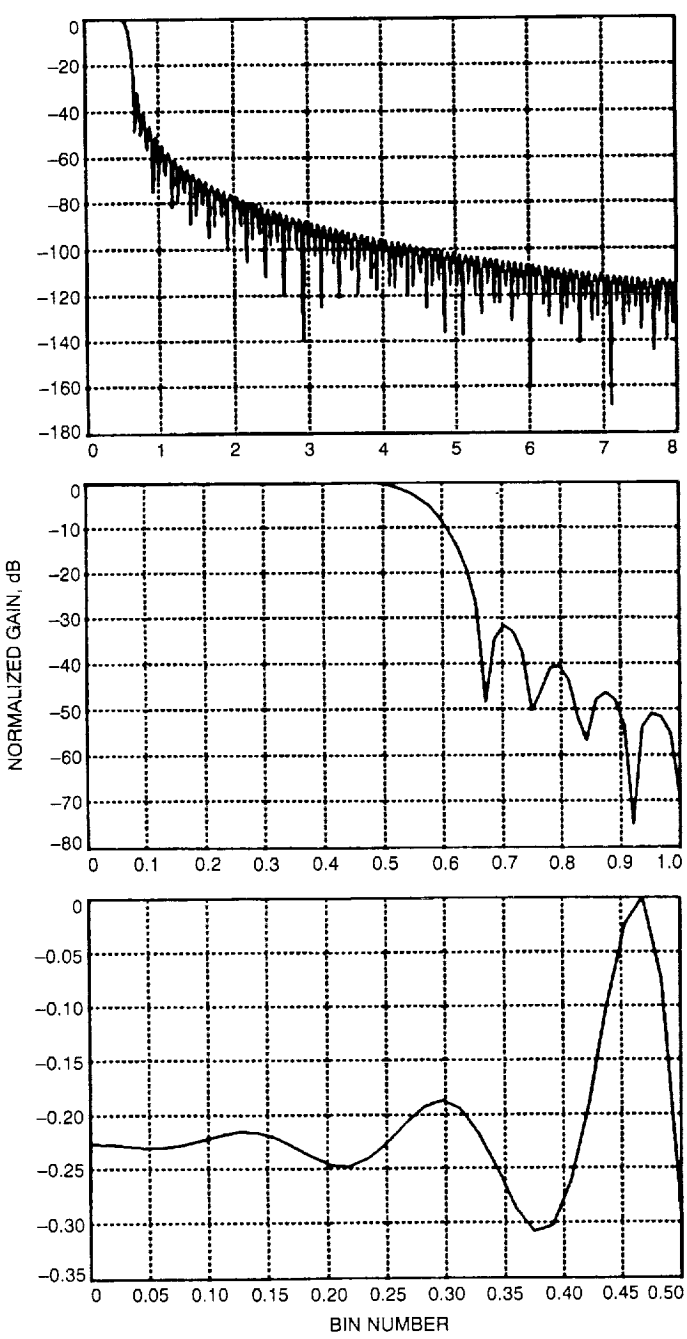

Fig. 13. Sample response with two close-up views of a 12-tap, 0.585-bin Parzen smoothed lowpass filter.

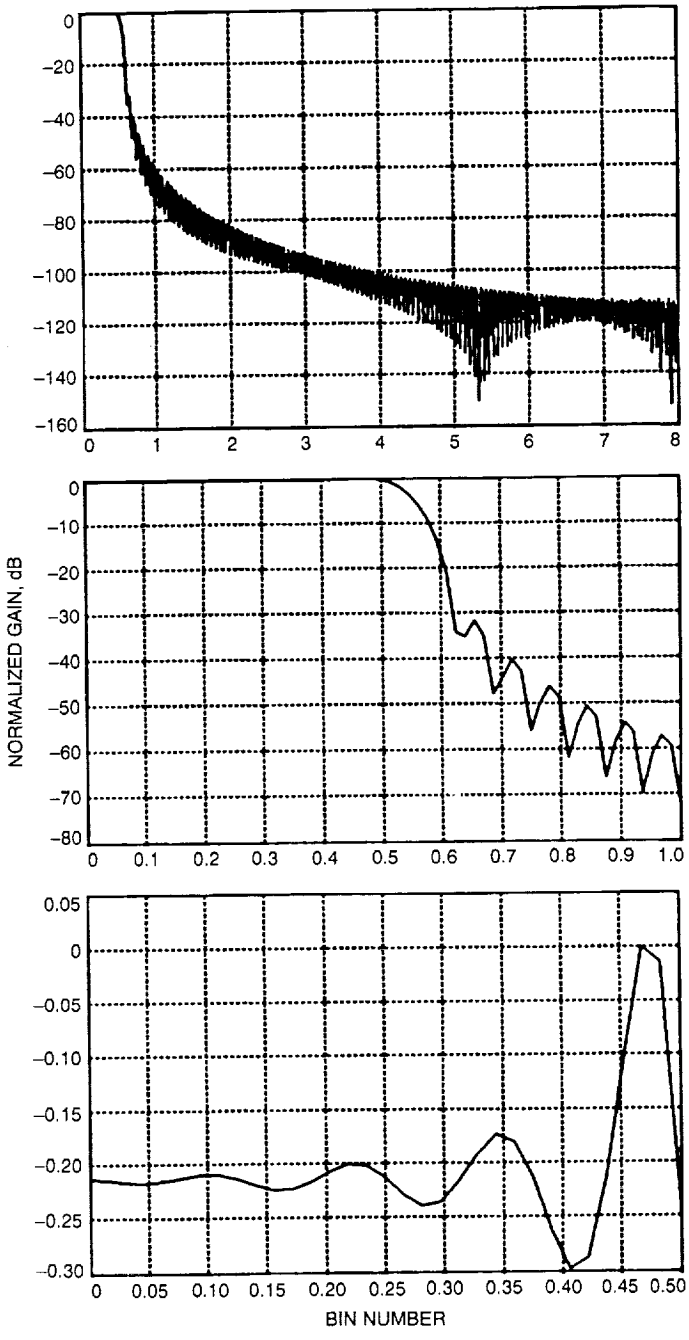

Fig. 14. Sample response with two close-up views of a 16-tap, 0.565-bin Parzen smoothed lowpass filter.

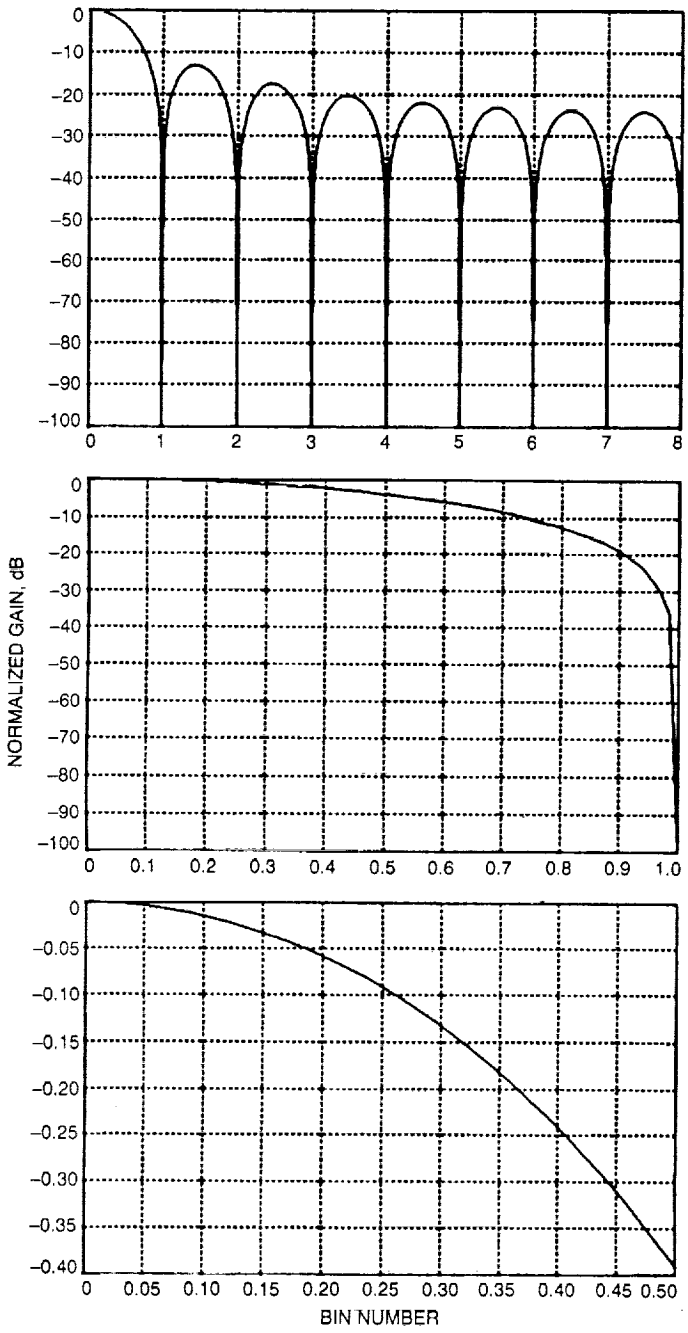

Fig. 15. Sample response with two close-up views of a rectangular window.

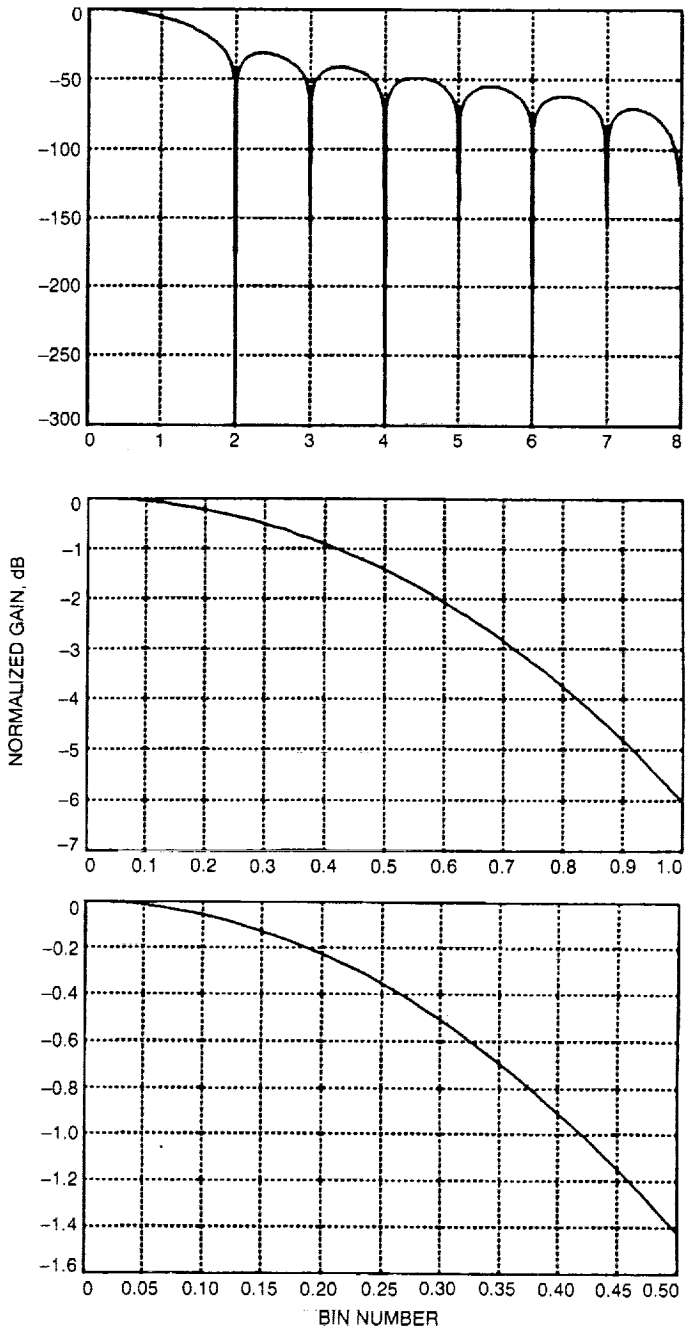

Fig. 16. Sample response with two close-up views of a Hanning window.